EASR

Engineering and Applied Science Research

https://www.tci-thaijo.org/index.php/easr/index

Published by the Faculty of Engineering, Khon Kaen University, Thailand

# Comparative adsorption study of Pb(II), Fe(II), and Zn(II) using non-chemically activated rubber seed shell biochar and commercial activated carbon

Chuthamat Chiamsathit[1)], Wittawat Toomsan[2)], Phadungsak Khomyos[1)], Surasak Thammarakcharoen[1)], Waraporn Khotwangouan[1)], Kraisorn Phukaew[1)], Wannatida Yonwilad[3)] and Pongsatorn Taweetanawanit*[1)]

[1)]Faculty of Health Science and Technology, Kalasin University, Kalasin 46230, Thailand
[2)]Nanotechnology Center (NANOTEC), National Science and Technology Development Agency (NSTDA), Pathum Thani 12120, Thailand
[3)]Faculty of Education and Educational Innovation, Kalasin University, Kalasin 46230, Thailand

Received 24 April 2025
Revised 23 September 2025
Accepted 1 October 2025

**Abstract**

The widespread contamination of water sources by heavy metals such as Pb(II), Fe(II), and Zn(II) poses serious environmental and health risks. This study investigated the use of non-chemically activated biochar derived from rubber seed shells, an agricultural waste material, as a sustainable adsorbent for heavy metal removal. Biochars were produced by a two-step carbonisation process at temperatures of 850, 900, and 950 °C, and the physicochemical properties were systematically assessed. The sample carbonised at 850 °C (PRC850) exhibited the most favourable properties, including a high BET surface area (795 m²/g), mesoporous structure, and suitable surface functional groups, as confirmed by SEM, BET, XRD, and FTIR analyses. Initial screening was conducted for Pb(II), Fe(II), and Zn(II) adsorption, and PRC850 demonstrated superior performance, removing up to 98.64% of Pb(II), which was significantly higher than the 85.52% removal rate achieved by commercial-grade activated (CGA) carbon. The adsorption behaviour of Pb(II) was best described by the Langmuir isotherm model, and the pseudo-second-order kinetic model fitted the experimental data well, indicating chemisorption. These findings indicated that rubber seed shell biochar had the potential to serve as a cost-effective and ecologically friendly adsorbent, particularly for Pb(II) removal, while also performing effectively for Fe(II) and Zn(II).

**Keywords:** Adsorbent, Adsorption, Biochar, Heavy metal, Rubber seed shell

## 1. Introduction

The issue of heavy metal contamination in water resources is widely recognised as a significant global environmental concern. Naturally occurring heavy metals are commonly found in both surface and groundwater, resulting in inherent contamination at relatively low concentrations. However, large volumes of wastewater from sources as diverse as factories, farms, landfills, hospitals, and municipalities have been discharged into natural water supplies and soils. The presence of pollutants in water leads to the contamination of drinking water, rendering it unfit for both consumption and domestic purposes [1]. High concentrations of iron (Fe), manganese (Mn), and zinc (Zn) have been observed in the groundwater supplies of both rural areas and hillsides in Thailand [2, 3]. Heavy metals are essential for industrial production, and as a result, industrial effluents tend to contain elevated levels of these elements. Some heavy metals, such as chromium (Cr), copper (Cu), lead (Pb), and cadmium (Cd), are widely used in a variety of industries including the chemical, distillery, tannery, textile, battery, pigment, hair dye, and petroleum sectors [4-6]. Although industrial factories are required to comply with environmental regulations and implement wastewater treatment systems, several reports have indicated that heavy metal contamination continues to occur due to system inefficiencies, improper operation, illegal discharges, or accidental leaks—particularly in small and medium-sized enterprises (SMEs) or in regions with limited regulatory enforcement. For example, in Thailand, elevated concentrations of Fe, Mn, Zn, Pb, and Cd have been detected in groundwater and surface waters near agricultural and industrial zones, even in areas where treatment systems are reportedly in place [7, 8]. Similarly, international studies have highlighted the residual presence of heavy metals in treated effluents due to the limitations of conventional treatment technologies and the cumulative impact of low-level discharges over time [9, 10]. Furthermore, naturally occurring heavy metals from geological formations can leach into water sources, contributing to the overall contamination burden. These findings justify the continued development of effective and affordable adsorbent materials for the removal of trace heavy metals, especially in contexts where conventional treatment alone does not guarantee complete removal.

Heavy metals present in water resources have non-biodegradable characteristics, leading to their subsequent transmission within the food chain. Hence, the phenomenon of heavy metal toxicity refers to the process through which metals accumulate in plants and animals through bioaccumulation. Heavy metals possess carcinogenic properties and pose significant harm to both human beings and other living organisms. In addition to naturally occurring sources and widespread industrial usage, there is increasing evidence that lead (Pb) contamination in water sources remains a pressing issue, particularly in developing countries. In Thailand, the Department

*Corresponding author.
Email address: Pongsatorn.ta@ksu.ac.th
doi: 10.14456/easr.2026.1

of Pollution Control reported measurable Pb concentrations in both surface water and sediments collected from urban canals and agricultural drainage basins near industrial zones [11]. Furthermore, a study found that Pb levels in shallow groundwater around informal e-waste recycling sites exceeded WHO drinking water guidelines [12]. Lead (Pb) is extensively utilised in several industries such as battery and accumulator manufacturing, dyeing silk yarn [13], paint production, the petrochemical sector for plastic stabilisation, and as an explosive detonator, among other purposes [14]. Pb is widely recognised as one of the most perilous elements owing to its high level of toxicity. Pb also has harmful consequences on human health, including anaemia and damage to bones, kidneys, and the brain [15, 16]. To achieve the permitted limit before discharging effluent into water resources or the environment, these heavy metals must be properly disposed of.

Heavy metals possess non-degradable characteristics; however, they can be effectively removed from water sources. Various practical techniques have been employed for the removal of chemical constituents and heavy metals, including electrodialysis, precipitation, membrane separation, electrocoagulation (EC), coagulation/flocculation, and filtration [17, 18]. While each method presents distinct advantages and limitations, a common challenge across these systems is the substantial generation of sludge, along with high energy consumption, significant capital investment, and considerable operational and maintenance costs [19]. Consequently, these methodologies tend to incur high costs. Adsorption is another widely used option for heavy metal removal due to its high removal efficiency and low operational and maintenance costs. Adsorption is widely used to remove organic and inorganic pollutants from water and air pollution [20, 21]. Many studies [22-24] have demonstrated that the adsorption approach is an effective technique for the elimination of heavy metals, typically utilised with commercial adsorbents and bio-adsorbents. The use of agricultural residue has been explored in adsorption methods as an environmentally sustainable means of removing heavy metals from water. In recent years, several research studies have investigated the development of cost-effective adsorbents incorporating biodegradable waste materials, including bio-carbon wastes [22], bamboo [23], rice husk [24], logan seed [25], rubber seed shell [26], cotton industry waste [27], and marigold flowers [28] as potential substitutes for activated carbon. The primary aim of this investigation was to evaluate the potential of rubber seed shell biochar for the adsorption of Pb(II), Fe(II), and Zn(II), as well as to examine the impact of various factors on the adsorption capacity, specifically for Pb(II). Due to its high level of toxicity, lead (Pb) is considered one of the most dangerous contaminants. Moreover, the presence of Pb in the environment has been shown to have detrimental impacts on human health, including the development of conditions such as anaemia, and the potential for organ damage to the skeletal structure, kidneys, and neurological functions [29]. In addition to lead, other metal ions such as iron (Fe) and zinc (Zn) are commonly detected in industrial and agricultural effluents. Although these metals are essential micronutrients, their elevated concentrations in water can pose environmental and health risks, including bioaccumulation and the disruption of aquatic ecosystems [2, 3, 24]. Therefore, Fe(II) and Zn(II) were included in the preliminary adsorption experiments in this study to provide a broader evaluation of the adsorbent's efficiency and to support the selection of the most promising material for further investigation of Pb(II) removal.

Despite the environmentally favourable nature of biosorption as a viable alternative to traditional approaches, the availability of commercialised adsorbents specifically designed for the removal of Pb(II) from water remains limited [30]. Future research should focus on identifying alternative adsorbents that address issues related to application, efficiency, and conventional limitations. The generation of activated carbon is typically achieved through physical or chemical activation process [31]. The use of physical activation techniques prior to other methods is more prevalent in industrial applications. These techniques enable the production of activated carbon at a reduced cost by employing readily available activating agents such as steam, carbon dioxide, or air [32, 33]. To produce activated carbon via chemical activation, agents such as $ZnCl_2$ and $H_2SO_4$ are used, and the process requires an acid-washing step as post-treatment to eliminate residual activating agent [34]. Nevertheless, the manufacture of activated carbon through physical or chemical activation involves substantial expenses, resource allocation, and extended production time. Avoiding activating agents during the synthesis of activated carbon can result in reduced production costs due to the lower cost of activating agents, elimination of post-treatment steps, and the absence of specialised facilities [35]. Therefore, it is crucial to develop a cost-effective manufacturing method for activated carbon that achieves a high degree of pore development, comparable to that obtained through physical and chemical activation. Further research is warranted to explore the activation of biochar at elevated carbonisation temperatures while excluding the use of activating agents. Hence, the current study was undertaken to conduct adsorption experiments to evaluate the effectiveness of adsorbents derived from non-chemical activated biochar sourced from rubber seed shells in the removal of Pb(II) from aqueous solutions.

This study evaluated the potential of rubber seed shells, which are by-products of rubber farms, as adsorbent materials. Numerous provinces and regions in Thailand contain expansive rubber plantations, making it one of the world's largest rubber producers. According to a reliable source [36], the quantity of rubber exports from Thailand during the first six months of the year was recorded at 2.19 million tonnes. Consequently, a substantial quantity of rubber seed shells remains scattered on the ground, giving rise to a challenge in waste management. Since the shells are commercially valuable, and are not used in agriculture applications, they are available for other uses such as biochar. Producing activated carbon using discarded agricultural waste or underused raw materials as adsorbents offers a potential solution to this issue [30]. The moisture content, ash content, bulk density, iodine number, and adsorption capacity of activated carbon are influenced by several factors, including the choice of raw materials, the activation methods used, and the processing conditions [37]. However, there is a lack of studies examining the production of activated carbon from Thai rubber seed shells. As a result, Thailand's rubber seed shells require further investigation as a potential source of raw material for the production of absorbent capable of removing heavy metal ions from water. The objective of this research was to investigate the properties and Pb(II) adsorption efficiency of adsorbents derived from non-chemical activated rubber seed shells biochar.

## 2. Materials and methods

### *2.1 Preparation of rubber seed shells*

Samples of rubber seed shells weighing over 10 kg were collected in Kalasin Province, Thailand. The rubber seed shells were typically characterised by their outer skin, commonly referred to as the husk. The removal of this outer layer required a meticulous process of peeling or scraping, usually performed using a knife or a similar tool. After the outer skin was removed, the shells were thoroughly cleaned by rinsing with clean water to eliminate any remaining soil or impurities. To separate unwanted materials or debris, the shells were sorted accordingly. The rubber seed shells underwent a washing process, followed by a 48-hour air-drying period. Subsequently, the shells were dried in an oven for 8 hours a temperature of 110 °C (see Figure 1a). A grinding machine was used to

pulverise the dried rubber seed shells into a fine powder (see Figure 1b), which was then sieved using a 150 µm mesh. The resulting material was stored in individual plastic containers.

(a) (b)

**Figure 1** Samples of rubber seed shells (a) dried rubber seed shells (b) ground rubber seed shell

*2.2 Preparation of the rubber seed shell adsorbents*

The methodology for producing rubber seed shell adsorbents using a non-chemical activated biochar technique is illustrated in Figure 2. The furnace temperature was maintained at 500 °C for two hours in the absence of oxygen. Subsequently, biochar was produced from rubber seed shells. The biochar was cooled to room temperature, sealed in a bag, and stored in a desiccator. The biochar samples were placed inside crucibles with lids and subjected to activation through carbonisation. Activation was achieved by heating the samples for 4 hours in an oxygen-limited muffle furnace. The activation process was conducted at three temperatures—850 °C, 900 °C, and 950 °C—at a heating rate of 10 °C/min. The activated carbon products were labelled PRC850, PRC900, and PRC950, and stored in a sealed container, which was then placed in a desiccator after cooling to room temperature.

The two-step carbonisation method was adopted to enhance the structural and adsorptive properties of the rubber seed shell biochar. The first stage, conducted at 500 °C for 2 hours in the absence of oxygen, served primarily to remove volatile matter and moisture while partially decomposing organic components. This step minimised thermal shock and helped preserve the physical framework of the biomass, which was important for maintaining structural stability during the subsequent activation stage [31, 32]. In the second stage, the biochar was subjected to high-temperature carbonisation at 850 °C, 900 °C, and 950 °C for 4 hours under limited oxygen conditions. This physical activation step promoted the development of a well-developed pore structure and high surface area, which were essential characteristics for effective adsorption [32, 33]. Unlike chemical activation methods that required corrosive agents and post-washing steps [34], this non-chemical activation approach eliminated the need for acid treatment and additional purification processes, thereby simplifying production and reducing environmental impacts. Although the method involved two heating steps, the overall energy demand was offset by the exclusion of energy-intensive chemical treatments, washing, and drying stages. Similar approaches were reported as cost-effective and scalable for biomass-derived activated carbon production [31, 35].


**Figure 2** Schematic illustration for the rubber seed shell adsorbents

*2.3 Description of commercial-grade adsorbent*

A granular commercial-grade activated (CGA) (Figure 3) carbon with a specified iodine number of 900 mg/g was used as a reference adsorbent in this study. The product was manufactured from bituminous coal via a two-step thermal activation process. Initially, the raw material was carbonised at low temperatures (200–300 °C) to remove volatile matter and moisture. It was then subjected to high-temperature steam activation (900–1000 °C) under controlled conditions. The CGA was purchased from a local supplier in Thailand. Prior to use, it was washed with distilled water, air-dried for 48 hours, oven-dried at 110 °C for 8 hours, and stored in a desiccator.

**Figure 3** Commercial-grade adsorbent (CGA)

*2.4 Physical characterisation of the adsorbents*

Physical characterisation analysis included various parameters of activated carbon, such as bulk density, iodine number, ash content, moisture content, and volatile matter. In this investigation, experiments were conducted in triplicate (n = 3) for each biochar sample. All studies were carried out in the laboratories of the Faculty of Health Science and Technology, located in Kalasin, Thailand. The findings of the investigation were subsequently compared to the standardised quality parameters of activated carbon. Table 1 presents the standards for activated carbon quality, as outlined in the Thai Industrial Standard (TIS No. 900-2547) [38].

**Table 1** Reference standard of activated carbon

| No. | Parameters | Unit | Reference Standard |
|---|---|---|---|
| 1 | Moisture content | wt% | ≤ 8 |
| 2 | Ash content | wt% | ≤ 10 |
| 3 | Bulk density | g/cm$^3$ | 0.25 – 0.75 |
| 4 | Iodine number | mg/g | ≥ 600 |

*2.4.1 Moisture content*

The American Society of Testing and Materials (ASTM D 2867-23) was used to measure the moisture content of the activated carbon [39]. Although the material used in this study was technically a biochar obtained via non-chemical physical activation, the standard method for determining moisture content was based on ASTM D 2867-23, which was originally designed for activated carbon. The application of this method was justified by its relevance and suitability for assessing the moisture content of porous carbonaceous materials, including biochar. Therefore, the term "activated carbon" appeared in the standard reference, while the analysis was conducted specifically on the biochar samples produced from rubber seed shells in this study.

One gram of biochar was placed in a porcelain evaporation dish and dried at 150 °C until the weight remained constant (approximately 3 hours). The weight of the sample was recorded after the porcelain evaporation dish containing the biochar was cooled to room temperature in a desiccator. The moisture content was calculated using the following equation:

$$\text{Moisture content (\%)} = \left[\frac{m_i - m_t}{m_i}\right] \times 100 \quad (1)$$

where $m_i$ and $m_t$ were the initial mass of the sample (g) and the mass of the dried sample (g), respectively.

*2.4.2 Ash content*

The American Society of Testing and Materials Standard (ASTM D 2866-11) was used to determine the ash content of activated carbon [40]. The biochar sample was dried at a temperature of 150 °C for approximately 3 hours until a constant weight was achieved. A dried sample weighing one gram was placed into a porcelain evaporating dish. The dish content were then combusted at 650 °C until the sample was completely converted into ash. The dish, along with the ash, was allowed to cool for approximately three hours before being weighed, yielding the same weight as before the combustion process. The porcelain evaporating dish was subsequently cooled to room temperature in a desiccator and weighted to determine the mass of biochar ash. The ash content was calculated using the following equation:

$$\text{Ash content (\%)} = \left[\frac{m_{ash}}{m_i}\right] \times 100 \quad (2)$$

where $m_i$ and $m_{ash}$ were the mass of the dried biochar sample (g) and the mass of the ash (g), respectively.

*2.4.3 Bulk density*

The American Society of Testing and Materials guidelines (ASTM D 2854-09) were used to analyse the bulk density of activated carbon [41]. Bulk density referred to mass of air-activated carbon per unit volume, including both the porous structure and the empty spaces between the particles. After three hours of drying at a constant weight between 110 °C and 120 °C, the biochar sample was cooled to room temperature in a desiccator. Initially, the 10 mL cylinder was weighed. The biochar sample was then placed into the cylinder by tapping its side, away from the prevailing air. Subsequently, the final weight was recorded. The bulk density was calculated using the following equation:

$$\text{Bulk density (g/cm}^3\text{)} = \frac{M}{V} \quad (3)$$

where *M* and *V* were the mass of the biochar sample (g) and the volume of the cylinder (mL), respectively.

*2.4.4 Volatile matter*

The American Society of Testing and Materials guidelines (ASTM D 5832-98) were used to analyse the volatile matter content of activated carbon [42]. A quantity of biochar weighing up to 1 gram was measured and subjected to a temperature of 950 °C in a furnace. After reaching the target temperature, the sample was held in the furnace for seven minutes to cool, ensuring that it remained isolated from external air contact. After the temperature was reduced, the desiccant was weighed. The volatile matter was calculated using the following equation:

$$\text{Volatile matter (\%)} = \left[\frac{m_i - m_t}{m_i}\right] \times 100 \quad (4)$$

where $m_i$ and $m_t$ were the initial mass of the sample (g) and the mass of the dried sample (g), respectively.

*2.4.5 Iodine number*

The iodine number represented the amount of iodine adsorbed from an aqueous solution, expressed in mg. Using a sample and a rapid test, iodine number analysis was used to determine the internal surface area of the activated carbon. In accordance with the American Society of Testing and Materials Standard (ASTM D 4607-14), the iodine number of activated carbon was measured [43]. The biochar sample was heated at 120 °C for three hours in an oven, followed by cooling to room temperature in a desiccator.

An Erlenmeyer flask with a 250 mL volume was filled with 0.5 g of biochar and 10 mL of 5% HCl. After boiling for 30 seconds, the liquid was allowed to cool to room temperature. The mixture was then added to a 100 ml solution of iodine at a concentration of 0.1 N (0.1 mol/L), followed by stirring for a duration of 30 seconds. The solution was subsequently filtered. A 50 mL portion of the filtrate was titrated with 0.1 N sodium thiosulphate until the yellow colour was nearly removed. After the addition of 1 mL of starch solution, the titration continued until the blue colour completely disappeared. The volume of sodium thiosulfate used was recorded.

The iodine number (X/M) was calculated using the following equations:

$$\frac{X}{M} = \frac{A - (DF \times B \times S)}{M} \quad (5)$$

$$A = N_2 \times 12693.0 \quad (6)$$

$$B = N_1 \times 126.93 \quad (7)$$

$$DF = \frac{(I + H)}{F} \quad (8)$$

where *X/M* is the iodine adsorbed per gram of carbon (mg/g), *DF* is the dilution factor, *I* is the volume of iodine (ml), *H* is the volume of 5% hydrochloric acid used (mL), *F* is the volume of filtrated solution (mL), $N_1$ is the normality of sodium thiosulfate (N), $N_2$ is the normality of iodine (N), *S* is the volume of sodium thiosulfate (mL), and *M* is mass of biochar used (g).

*2.5 Elemental and surface morphology analyses of adsorbents*

A scanning electron microscope (SEM, Hitachi, Model: S-3400N, Japan) was used in this investigation to characterise the surface morphology of the biochar derived from rubber seed shells. The surface area of the samples was determined using the Brunauer–Emmett–Teller (BET) technique, which involved analysis of the $N_2$ adsorption–desorption isotherm at a temperature of 77 K, using the Quantachrome NOVA2000e instrument. X-ray diffraction (XRD) analysis was performed using an X-ray diffractometer (Bruker, Model: D8 Advance) operating at 40 kV and 40 mA, with Cu Kα radiation.

The surface chemistry of biochar samples was analysed using Fourier transform infrared (FTIR) spectroscopy, specifically the Thermo Scientific Nicolet iS50 instrument. The biochar samples were prepared by mixing 0.25 mg of each sample with 100 mg of potassium bromide (KBr). Each mixture was then compressed using a manual hydraulic press at a pressure of 2 MPa for 3 minutes, resulting in the formation of a thin, translucent disc. The FTIR spectra were recorded in the wavenumber range of 4000 to 400 $cm^{-1}$ at a resolution of 4 $cm^{-1}$. Spectra were obtained in transmission mode, with 32 scans performed for each run.

*2.6 Adsorption studies*

Distilled water was used to prepare a stock solution containing 1000 mg/L of Pb (II), Fe (II), and Zn (II). This stock solution was then used to prepare dilutions for the adsorption tests. All adsorption experiments were conducted in 250 mL Erlenmeyer flasks containing 100 mL of the prepared solution. Each solution was further treated with 20 mL of 0.5 M $HNO_3$. Three parallel experiments, along with a control, were carried out for each measurement. The concentration of Pb, Fe, and Zn were measured using an atomic absorption spectrometer (AAS-PinABCLe 900F).

*2.6.1 Effect of different adsorbent*

The adsorption capacity of the heavy metal solutions were examined at various carbonisation temperatures of biochar (800 °C, 850 °C, and 950 °C) in order to determine the influence of carbonisation temperature. In a 250 mL Erlenmeyer flask, 100 mL of each solution containing 0.5 mg/L Pb (II), 0.5 mg/L Fe (II), and 0.1 mg/L Zn (II) was mixed with 1 g of biochar. The flasks were placed in a vapour bath and shaken continuously at 150 rpm for two hours at 30 ± 0.5 °C.

*2.6.2 Effect of adsorbent dosage*

Different amounts of adsorbent (0.5, 1, 2, 4, 8, and 16 g) were added to 100 mL of the 0.5 mg/L Pb (II) stock solution in order to examine the effects of biochar dosage. The comparison and investigation of the effects of commercial-grade activated carbon dosages were also conducted. The flasks were continuously shaken in a vapour-bathing vibrator at 150 rpm for 2 hours at 30 ± 0.5 °C.

*2.6.3 Effect of initial concentrations*

Adsorption isotherms were obtained by mixing 100 mL of Pb (II) solution with 0.5 g of adsorbent at various concentrations (ranging from 0.25 to 8.00 mg/L) in 250 mL Erlenmeyer flasks. The flasks were placed in a vapour-bathing vibrator and shaken continuously at 150 rpm for 2 hours at 30 ± 0.5 °C.

*2.6.4 Effect of contact times*

To conduct adsorption kinetics experiments, 0.5 g of adsorbent was weighed into a 250 mL Erlenmeyer flask along with 100 mL of a 0.955 mg/L Pb (II) stock solution. The mixture was agitated at 150 rpm for 30 minutes, 1 hour, 2 hours, 4 hours, and 6 hours at a temperature of 30 ± 0.5 °C. After each contact time, filter paper was used to remove the biochar from the mixture to obtain a sample solution. The concentration of heavy metals (mg/L) in the solution was measured using an atomic adsorption spectrometer (PinABCLe 900F).

The adsorption capacity ($Q_e$) and the removal efficiency ($E$) were calculated using the following equations:

$$Q_e = [\frac{C_i - C_t}{m}] \times v \quad (9)$$

$$E\ (\%) = [\frac{C_i - C_t}{C_i}] \times 100 \quad (10)$$

where $Q_e$ was the amount of heavy metal adsorbed per gram of biochar (mg/g), $C_i$ and $C_t$ were the initial and equilibrium concentrations of the heavy metal (mg/L), $v$ was the volume of the solution (L), and $m$ was the mass of biochar used (g).

*2.6.5 Adsorption isotherms*

Adsorption isotherms were used to describe the adsorption behaviour of a solute on the adsorbent at equilibrium under constant temperature conditions. Among all biochar samples tested, PRC850 demonstrated the highest adsorption efficiency for Pb(II), Fe(II), and Zn(II) under the same experimental conditions. Therefore, PRC850 was selected as the representative adsorbent for the isotherm study. This approach enabled a more accurate evaluation of adsorption behaviour using the Langmuir and Freundlich models, while minimising the influence of varying surface properties associated with different carbonisation temperatures.

As a result, the equilibrium experimental data for Pb, Fe, and Zn adsorption on PRC850 and CGA were fitted to two common isotherm models: the Langmuir and Freundlich isotherms, as shown in Eqs. (11) and (12), respectively:

$$q_e = \frac{Q_{max} \cdot b \cdot C_e}{(1 + b \cdot C_e)} \quad (11)$$

$$q_e = K_F \cdot C_e^{1/n} \quad (12)$$

where $C_e$ (mg/L) was the equilibrium concentration of Pb, Fe, and Zn in the aqueous phase, $Q_{max}$ (mg/g) was the maximum adsorption capacity based in the Langmuir equation, $b$ (L/mg) was the Langmuir constant, $K_F$ ($mg^{1-1/n}.L^{1/n}/g$) was the adsorption coefficient based on the Freundlich equation, and $1/n$ was the adsorption intensity based on the Freundlich equation.

*2.6.6 Adsorption kinetics*

To explore the adsorption kinetics of Pb (II), Fe (II), and Zn (II) ions onto PRC850 and CGA, the experimental kinetic data for heavy metal adsorption were fitted to linear pseudo-first-order (PFO) and pseudo-second-order (PSO) models, as shown in Eqs.13 and 14:

$$\ln(q_e - q_t) = \ln q_e - K_1 t \quad (13)$$

$$\frac{t}{q_t} = \frac{1}{K_2 q_e^2} + \left(\frac{1}{q_e}\right) t \quad (14)$$

where $q_e$ was the amount of Pb (II), Fe (II), and Zn (II) adsorbed at equilibrium (mg/g), $q_t$ was the amount adsorbed at time $t$ (mg/g), and $K_1$ and $K_2$ were the rate constants for the PFO (L/min) and PSO (g/mg·min), respectively.

## 3. Results and discussion

*3.1 Adsorbent characterisation*

The adsorbent material is depicted in Figure 4 at different carbonisation temperatures. The PRC850, PRC900, and PRC950 biochar samples appeared similar in both their physical characteristics and colouration. Table 2 presents the physicochemical parameters of PRC850, PRC900, and PRC950. The rubber seed shell adsorbents were characterised by their elevated iodine number, relatively minimal ash level, and diminished moisture content. The results presented in Table 2 were similar to those observed in the granular-

form commercial-grade adsorbent (CGA). Based on the results, it was determined that PRC850, PRC900, and PRC950 met the requirements outlined in the Thai Industrial Standard (TIS No. 900-2547) regarding their physical and chemical properties. Consequently, the adsorbents derived from rubber seed shells demonstrated satisfactory quality and were comparable to commercial-grade activated carbon.

Among all samples tested, PRC850 had the highest iodine number (725.70 mg/g), indicating the most developed microporous structure and high surface area among the biochar materials. This result suggested that carbonisation at 850 °C created optimal conditions for volatile matter release and pore development without causing excessive structural damage [15]. In contrast, PRC900 exhibited a higher volatile matter content (53.00%) but a lower iodine number (635.41 mg/g), implying that additional volatile compounds did not contribute to further pore formation. Meanwhile, PRC950 had the lowest volatile matter (38.37%) due to advanced thermal decomposition, but the iodine number slightly increased compared to PRC900 (659.61 mg/g), likely due to partial pore collapse at elevated temperatures [22].

The relatively high volatile matter content in PRC850 and PRC900 (47.57% and 53.10%, respectively) was attributed to the carbonisation process being conducted without nitrogen or inert gas purging. The absence of oxygen control likely resulted in incomplete devolatilisation and partial oxidation. Although hemicellulose typically decomposed below 350 °C and cellulose around 400–500 °C, lignin and its derivatives persisted and released volatiles gradually at temperatures beyond 500 °C, particularly under semi-controlled pyrolysis conditions. These characteristics were consistent with biochars derived from lignocellulosic biomass processed without inert atmospheres [44].

It was observed that the ash content of the rubber seed shell-derived adsorbents decreased slightly with increasing carbonisation temperature, from 2.21 wt% at 850 °C to 1.89 wt% at 950 °C. This trend was attributed to the volatilisation and decomposition of inorganic substances during high-temperature carbonisation. The inorganic residue in RSS was likely dominated by calcium and magnesium compounds, possibly in the form of oxides or carbonates (e.g. CaO, MgO, $CaCO_3$), as well as trace amounts of potassium, sodium, and silica. This study reported ash compositions of RSS carbon containing approximately 0.32% Ca and 0.673% Mg [45]. Such inert minerals were expected to persist through carbonisation at 850–950 °C. As temperature increased, more volatile inorganic compounds were likely released, leading to a lower residue of ash in the final product. This lower amount may have been due to the volatilisation of thermally unstable inorganic compounds, such as carbonates, which can decompose or evaporate at high temperatures. Moreover, the absence of nitrogen or inert gas during carbonisation may have promoted partial oxidation, contributing to a further reduction in ash content. This behaviour aligned with previous studies on biomass pyrolysis, which reported a reduction in ash content at elevated carbonisation temperatures due to the thermal instability of certain mineral components [25].

The bulk density of PRC850 was also the lowest (0.28 g/cm³), reflecting a more porous and lighter carbon matrix. This parameter increased slightly in PRC900 and PRC950 (0.30 g/cm³), likely due to the densification of the structure from heat-induced shrinkage. These physical properties supported the superior adsorption performance of PRC850 in subsequent experiments.

The percentage yield of PRC850, PRC900, and PRC950 was relatively consistent, ranging from 21.93 ± 0.06% to 21.98 ± 0.04%, indicating minimal influence of carbonisation temperature within the 850–950 °C range under the applied pyrolysis conditions. The biochar yields of PRC850–950 (~22%) fell within the typical range for lignocellulosic biomass subjected to high-temperature pyrolysis. This consistency across 850–950 °C suggested that most thermally labile components such as cellulose and hemicellulose had already decomposed at 850 °C, leaving lignin-rich structures that were more resistant to further degradation.

Higher carbonisation temperatures were generally associated with enhanced porosity and surface area but reduced mass recovery, as observed in previous studies where pyrolysis at 850 °C of softwood produced a high surface area of 764 m²/g but yielded only ~15% of biochar [45]. Similarly, slow pyrolysis of woody and non-woody biomass at 500–600 °C resulted in yields of 23.46–25.98%, indicating that higher temperatures led to greater volatile release and lower product yield [46]. The absence of a yield value for CGA was due to its status as a commercially activated carbon product, for which raw mass and processing data are not typically disclosed to end users.

Hence, these adsorbents were suitable for the extraction of heavy metal ions from aqueous solutions. However, PRC850 should be prioritised in biochar manufacturing due to its high iodine number and low carbonisation temperature.


**Figure 4** Biochar produced from rubber seed shells at three different carbonisation temperatures: (a) PRC850, (b) PRC900, and (c) PRC 950 (Note: The image of CGA was shown in Figure 3, as it was not included in the biochar production process.)

**Table 2** Physicochemical properties of adsorbents

| Parameters | Unit | PRC850 | PRC900 | PRC950 | CGA |
|---|---|---|---|---|---|
| Moisture content | wt% | 0.15±0.02 | 0.10±0.01 | 0.10±0.01 | 0.13±0.01 |
| Ash content | wt% | 2.21±0.15 | 2.17±0.21 | 1.89±0.22 | 1.06±0.15 |
| Bulk density | g/cm$^3$ | 0.28±0.01 | 0.30±0.02 | 0.30±0.02 | 0.49±0.02 |
| Volatile matter | % | 47.57±7.16 | 53.10±5.53 | 38.47±4.84 | 15.33±0.76 |
| Iodine number | mg/g | 725.70±44.53 | 635.41±47.47 | 659.61±34.92 | 790.86±19.61 |
| Yield | % | 21.93±0.06 | 21.96±0.04 | 21.98±0.04 | N/A |

*3.2 Elemental and surface morphology analyses*

*3.2.1 SEM analysis*

Figure 5 displays SEM images of porous carbon materials CGA and PRC850. The results indicated that the morphology of CGA was slightly more compact than that of PRC850. Nevertheless, the compositions of both adsorbents consisted of thin layers exhibiting various shapes and sizes. The SEM image of CGA (Figure 5a) showed an agglomerated and disordered particle structure with a relatively compact surface, which may have limited the exposure of active adsorption sites. In contrast, PRC850 (Figure 5b) exhibited a more open and layered morphology, with sheet-like structures and clear gaps between the layers.

This transformation in morphology suggested that the carbonisation process at 850°C significantly enhanced the porosity and surface accessibility of the carbon material, which was advantageous for adsorption applications. The structural differences observed in the SEM images were further supported by the physicochemical data presented in Table 2 and correlated well with the adsorption performance of each sample.

Although CGA had a higher iodine number (790.86 mg/g), its relatively high bulk density (0.49 g/cm³) and compact, agglomerated surface morphology (Figure 5a) suggested restricted internal porosity and limited accessibility to active sites. In contrast, PRC850, despite having a slightly lower iodine number (725.70 mg/g), demonstrated a significantly more open, layered, and porous microstructure (Figure 5b). This structure was consistent with its lower bulk density (0.28 g/cm³) and higher volatile matter content (47.57%), indicating the development of a less dense carbon framework with more accessible pore volume.

The SEM image clearly showed well-separated sheets and surface voids, which likely facilitated better diffusion and interaction with heavy metal ions during adsorption.

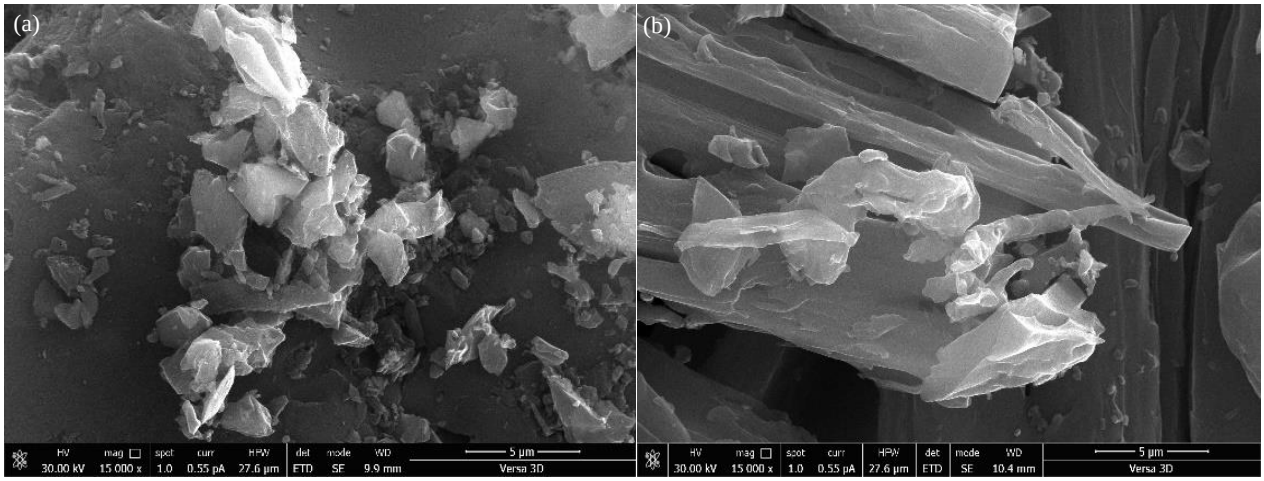


**Figure 5** SEM images of activated carbon samples: (a) CGA and (b) PRC850

*3.2.2 Surface area analysis*

The $N_2$ adsorption-desorption test was used to further examine the BET surface areas and pore size distribution of the layered CGA and PRC850. The BET-specific surface areas of CGA and PRC850 were measured and found to be 925 and 795 $m^2/g$, respectively.

To further evaluate the adsorption performance and surface characteristics of PRC850, comparisons were made with other adsorbents reported in recent studies. The BET surface area of PRC850 was found to be 795 m²/g, which was significantly higher than that of rice husk-based activated carbon (253.4 m²/g) [24], and moderately lower than that of longan seed-based activated carbon prepared by NaOH activation (975.18 m²/g) [25].

The pore size distribution data (Figure 6) revealed that PRC850 possessed a predominantly mesoporous structure, with pore diameters ranging from 3 to 60 nm and the majority centred within the 3–8 nm range. In contrast, CGA showed a broader distribution of pore sizes, extending from 3 to 138 nm, with most pores falling within the 17–138 nm range, indicating a larger contribution from macropores.

Although CGA exhibited a higher total pore volume at larger diameters (notably beyond 60 nm), these macropores were generally less favourable for the effective adsorption of small-sized heavy metal ions such as Pb(II), Fe(II), and Zn(II), which require more accessible surface areas and confined pore environments for strong interaction.

In comparison, the mesoporous structure of PRC850 enhanced both surface accessibility and diffusion kinetics, allowing more efficient interaction with heavy metal ions, especially Pb(II) [25]. This observation supported the superior adsorption capacity of PRC850 over CGA despite its slightly lower BET surface area (795 m²/g vs. 925 m²/g).

The presence of a well-developed mesoporous network in PRC850 facilitated capillary condensation and promoted multilayer adsorption processes, both of which were advantageous in the adsorption of ionic contaminants from aqueous systems [47, 48]. Previous studies similarly reported that mesoporous carbon structures, particularly those in the 2–10 nm range, exhibited enhanced adsorption for heavy metals due to a combination of pore confinement, surface chemistry, and electrostatic interactions [44].

These findings suggested that PRC850 provided a sufficiently high specific surface area for effective adsorption, despite being produced via a non-chemical activation method.

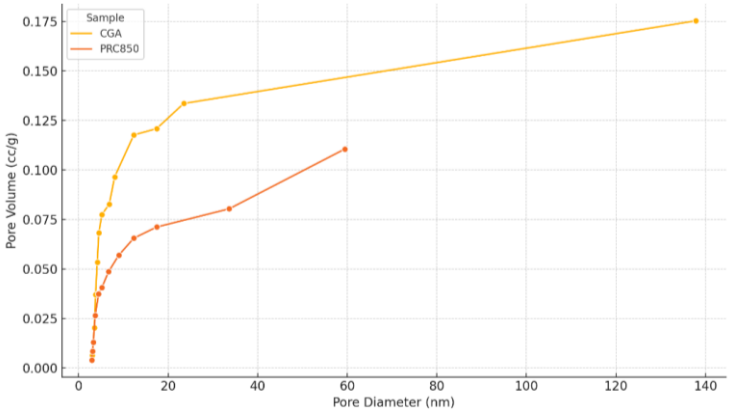


**Figure 6** Pore size distribution of PRC850 and CGA, determined by nitrogen adsorption–desorption analysis using the BJH method

*3.2.3 XRD analysis*

The X-ray diffraction (XRD) technique was used to conduct structural characterisations of CGA and PRC850. The outcomes of these characterisations supported the morphological observations, shown in Figure 7. Both adsorbents exhibited two prominent and broad diffraction peaks centred at approximately $2\theta = 24°$ and $2\theta = 42°$, which were attributed to the (002) and (100) crystallographic planes of amorphous carbon, respectively. These broad peaks were characteristic of disordered carbon structures with low graphitisation, commonly found in biochar and physically activated carbon derived from lignocellulosic biomass [49].

In the case of PRC850, a single sharp peak was observed at approximately $2\theta = 27°$. This peak may have indicated partial alignment or structural ordering of carbon layers induced by high-temperature carbonisation at 850°C. This may also have correspond to the presence of trace quartz ($SiO_2$) impurities, as the (011) crystallographic plane of quartz exhibited diffraction near 26.6–27° [50]. This observation suggested the possible presence of mineral residues from the raw biomass.

The absence of a distinct diffraction peak near $2\theta = 22°$, typically associated with crystalline cellulose, suggested that most of the cellulose content was thermally decomposed during carbonisation at 850 °C [51, 52]. This featured aligned with the thermal degradation behaviour of cellulose, which usually decomposes below 400 °C. Thus, the broad amorphous halo at 24° was more likely related to disordered carbon structures than to residual cellulose.

The complete thermal decomposition of cellulose in rubber seed shell biochar at 850 °C had notable implications for both volatile matter and ash content. Since cellulose typically degrades within the range of 315–400 °C [53], its absence in PRC850 indicated that the remaining volatile matter (47.57%) was primarily derived from more thermally stable components, such as lignin, which degrades over a broader temperature range (200–700 °C) [54], or condensed aromatic intermediates. These compounds decomposed more slowly, particularly under non-inert pyrolysis conditions without nitrogen purging, where partial oxidation may have further modified the release patterns of volatile species [55].

In contrast, the XRD pattern of CGA displayed multiple distinct peaks, notably at approximately $2\theta = 20°$ and 27°. The peak at $2\theta = 20°$ was typically associated with amorphous silica or cellulose remnants, while the 27° peak may also have been attributed to quartz or other crystalline minerals introduced during chemical activation or processing. These sharper peaks suggested the presence of crystalline inorganic phases or additives that were often incorporated in commercial-grade activated carbon during manufacturing.

Overall, the broad diffraction features and lack of well-defined crystalline peaks in both PRC850 and CGA confirmed their predominantly amorphous nature. The differences in peak intensities and positions further reflected variations in mineral content, carbon ordering, and processing methods between the two materials. These findings were consistent with the SEM and BET results, which indicated that PRC850 exhibited a porous, disordered carbon structure favourable for heavy metal adsorption.

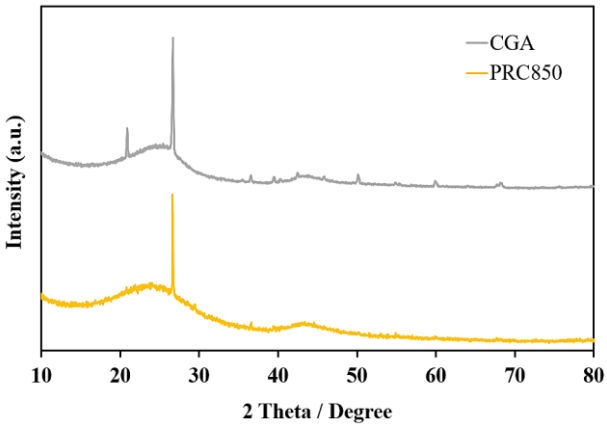


**Figure 7** X-ray diffraction (XRD) patterns of CGA and PRC850

*3.2.4 FTIR analysis*

The Fourier transform infrared (FTIR) spectra of CGA and PRC850 are shown in Figure 8. According to the FTIR spectra, PRC850 exhibited minimal dissimilarities compared to CGA. The CGA sample displayed several prominent absorption bands indicative of

oxygen-containing functional groups derived from the raw biomass precursor. Table 3 presents peak wavenumbers and functional groups of CGA and PRC850.

CGA exhibited prominent peaks at 3425 $cm^{-1}$ (–OH stretching), 2924 $cm^{-1}$ (C–H stretching), and 1710 $cm^{-1}$ (C=O stretching), indicating the presence of hydroxyl, aliphatic, and carbonyl groups originating from the original biomass. Additional bands at 1635 $cm^{-1}$ and 1062 $cm^{-1}$ corresponded to aromatic C=C and C–O stretching, respectively.

In contrast, the FTIR spectrum of PRC850 revealed significant reduction or complete disappearance of the aforementioned bands. The decrease in O–H and C–H stretching vibrations indicated the decomposition of volatile organic matter and dehydration during carbonisation. The C=O stretching band at 1710 $cm^{-1}$ also vanished, suggesting the removal of carboxylic and carbonyl functionalities due to decarboxylation reactions under high-temperature treatment.

The overall spectral profile of PRC850 became smoother, with fewer distinct peaks, indicating a more condensed, aromatic, and less functionalised carbon structure. This transformation suggested a shift toward a hydrophobic, graphitised structure with fewer polar sites, which may have enhanced structural stability and adsorption efficiency. The adsorbents acquired an increased surface area, thereby augmenting the adsorption of $CO_2$ [26].

**Table 3** Peak wavenumbers and functional groups of CGA and PRC850

| Wavenumber ($cm^{-1}$) | Functional Group | Vibration Mode | CGA (Raw Carbon) | PRC850 (850 °C) |
|---|---|---|---|---|
| 3425 | Hydroxyl (–OH) | O–H stretching (H-bonded) | Strong & broad | Significantly reduced |
| 2924 | Aliphatic C–H | C–H stretching ($CH_2$, $CH_3$) | Moderate | Disappeared or very weak |
| 1710 | Carbonyl (C=O) | C=O stretching (carboxyl, ketone) | Sharp | Absent |
| 1635 | Aromatic C=C | C=C skeletal stretching (aromatic) | Present | Weak |
| 1062 | C–O (ether, alcohol) | C–O stretching | Moderate | Weak |

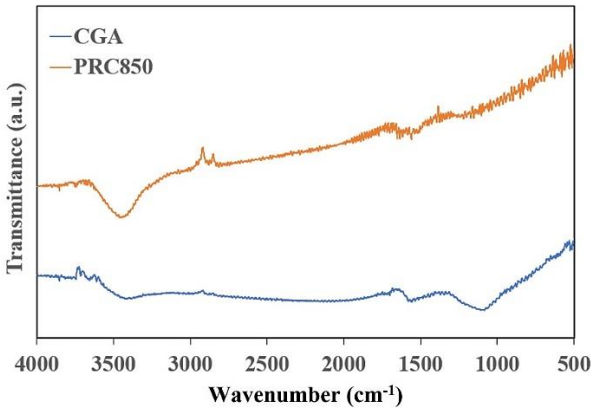


**Figure 8** FTIR analysis of the CGA and PRC850

*3.3 Initial evaluation of adsorbents*

The initial adsorption tests were performed on heavy metal ions, specifically Pb(II), Fe(II), and Zn(II), using rubber seed shell adsorbents produced at varying carbonisation temperatures (850 °C, 900 °C, and 950 °C). The adsorption capacities of Pb(II), Fe(II), and Zn(II) on commercial-grade adsorbent (CGA) were determined and found to be 46.13 mg/g, 43.93 mg/g, and 10.73 mg/g, respectively.

Figure 9 depicts the variation in adsorption capacity of Pb(II), Fe(II), and Zn(II) on rubber seed shell biochar as a function of carbonisation temperature. The ability of rubber seed shell adsorbent to remove Zn(II) from a single aqueous solution increased as the carbonisation temperature increased. This phenomenon may have been associated with thermal modifications of the carbon surface or the formation of larger pore channels, which could have enhance Zn(II) diffusion and interaction, even though microporosity (as indicated by iodine number) slightly decreased.

Nevertheless, it was observed that the carbonisation temperature of 950 °C exhibited the greatest adsorption capacity for Zn(II), reaching 62.97 mg/g. Furthermore, it was noted that as the carbonisation temperature increased, the rate at which the adsorption capacity reached a steady state became slower. Therefore, producing activated carbon from rubber seed shells at a carbonisation temperature of 900 °C (PRC900) was considered appropriate for removing Zn(II) (62.43 mg/g).

Nonetheless, it was observed that the adsorption efficiencies of Pb(II) and Fe(II) experienced a slight decrease with increasing carbonisation temperature. This trend could be attributed to the attainment of equilibrium in the contact surface area of the adsorbent particles at a temperature of 850 °C.

As a result, it can be shown that the carbonisation temperature of 850 °C exhibited the most effective adsorption efficiency for Pb(II) (51.07 mg/g) and Fe(II) (49.13 mg/g). Hence, the use of rubber seed shell adsorbent at a carbonisation temperature of 850 °C (PRC850) appeared appropriate for the elimination of Pb(II) and Fe(II). As a result, the PRC850 exhibited higher performance compared to CGA in the removal of Pb(II), Fe(II), and Zn(II).

Previous studies on the adsorption capacity of Pb(II) showed that bamboo adsorbent achieved a rate of about 37 mg/g [23], rice husk adsorbent achieved a rate of about 6 mg/g [24], and avocado seed achieved a rate of about 79.3 mg/g [15].

In terms of adsorption performance, PRC850 demonstrated a Zn(II) adsorption capacity of 62.97 mg/g at an initial concentration of 0.1 mg/L, outperforming Nigerian bamboo-based activated carbon, which exhibited a maximum Zn(II) adsorption capacity of 20 mg/g at a higher initial concentration of 166 mg/L [23].

Moreover, PRC850 achieved Zn(II) removal efficiencies exceeding 60%, while rice husk-derived activated carbon showed approximately 70% Zn(II) removal and only 60% Pb(II) removal at the same adsorbent dosage of 0.5 g [24]. These comparisons highlighted the strong competitive performance of PRC850, especially considering that its preparation did not involve chemical activating agents or high-cost processing.

The findings from the initial assessment of rubber seed shell adsorbents in terms of their efficacy in removing Pb(II), Fe(II), and Zn(II) are depicted in Figure 10. All rubber seed shell adsorbents examined removed Pb(II) at rates above 90%, outperforming the CGA adsorbent. It is noteworthy that PRC850 demonstrated the highest Pb(II) removal efficiency, reaching 96%.

All the rubber seed shell adsorbents examined showed Fe(II) removal efficiencies greater than 82%, comparable to those of CGA, except for PRC950, which removed roughly 78% of the Fe(II).

The adsorption behaviour of heavy metal ions on biochar materials was strongly influenced by both physical and chemical mechanisms. Physical adsorption was primarily governed by the pore size distribution and surface area of the adsorbent, while chemical adsorption involved interactions with surface functional groups.

The ionic radii of Pb(II), Fe(II), and Zn(II) were approximately 119 pm, 78 pm, and 74 pm, respectively [56-58]. These dimensions were relatively small compared to the dominant mesopores of PRC850, which ranged between 3–8 nm (30–80 Å or 3000–8000 pm). Therefore, all three ions could easily diffuse through the porous structure of PRC850. The mesoporous architecture of PRC850 offered a balance between rapid diffusion (typical of macropores) and strong retention via capillary forces and confined environments (typical of micropores), which enhanced the physical adsorption of these ions.

The observed trend of adsorption efficiency—Pb(II) > Fe(II) > Zn(II)—could be attributed to the fundamental physicochemical properties of the metal ions. Pb(II), which possessed a larger ionic radius and lower hydration energy compared to Fe(II) and Zn(II), interacted more readily with the adsorbent surface [59]. Moreover, Pb(II) exhibited a higher affinity toward oxygen-containing functional groups such as –OH and –COOH, commonly present on biochar surfaces [60]. These properties enhanced this biochar's ability to form strong inner-sphere surface complexes via ion exchange or complexation mechanisms [61]. This preferential adsorption pattern was consistent with previous studies, which also reported a higher selectivity of carbon-based materials for Pb(II) in multi-metal systems due to its higher polarisability and stronger binding strength. All the examined rubber seed shell adsorbents were more effective at removing Zn(II) than CGA, with an average removal rate of over 60%.

The $N_2$ adsorption–desorption analysis was carried out to evaluate the specific surface area and porosity of CGA and PRC850. The BET-specific surface areas of CGA and PRC850 were measured to be 925 $m^2/g$ and 795 $m^2/g$, respectively. Despite CGA showing a higher surface area, it exhibited lower adsorption performance for Pb(II), Fe(II), and Zn(II) compared to PRC850. This performance suggested that surface area alone did not fully determine adsorption capacity; the accessibility and quality of the pore structure also played significant roles.

PRC850 possessed a dominant mesoporous structure, with pore sizes primarily in the range of 3–8 nm, which was well-suited for the diffusion and retention of heavy metal ions. Conversely, CGA exhibited a broader pore size distribution extending into the macroporous region (17–138 nm), which may have led to lower surface interaction efficiency due to reduced contact between the adsorbate and the active sites within the pores. This distribution could be attributed to its more open and layered morphology, as observed in SEM images, and its lower bulk density (0.28 $g/cm^3$), which indicated a more accessible porous network.

Furthermore, the higher volatile matter content (47.57%) of PRC850 suggested enhanced micropore development during the carbonisation process, facilitating greater ion diffusion and adsorption. When compared to other reported adsorbents, the surface area of PRC850 was significantly higher than that of rice husk-based activated carbon (253.4 $m^2/g$) [24] and moderately lower than that of longan seed-based activated carbon prepared by NaOH activation (975.18 $m^2/g$) [25].

These findings highlighted that PRC850 provided a high-efficiency adsorbent with environmentally friendly preparation, as it was synthesised without chemical activation yet achieved comparable or superior performance to chemically activated materials. Additionally, the carbonisation at 850°C for biochar from rubber seed shell likely promoted favourable pore structures and active sites that contributed to high adsorption efficiency across multiple metals.

To evaluate the removal efficiency of Pb(II), prior studies on activated carbon indicated that lignin-based porous carbon achieved a 96% removal rate [62], *Acanthospermum hispidum* weed achieved a 95% removal rate [63], and coconut shell achieved an 88% removal rate [64].

Compared to those chemically activated carbon studies, the PRC850 performed comparably to other bio-adsorbents and was superior to CGA at removing Pb(II). This removal was achieved with a reduced quantity of adsorbent, higher initial concentrations of Pb(II), shorter contact time, and under conditions that closely resembled natural environments. This enhanced performance was attributed to the unique surface morphology and functional groups developed during the physical activation process. Despite not employing chemical activating agents, PRC850 demonstrated a fibrous structure with accessible pores, as observed via SEM, and retained oxygen-containing surface groups such as hydroxyl and carboxyl groups, as confirmed by FTIR. These characteristics promoted effective complexation and electrostatic interaction with Pb(II) ions. Furthermore, the high removal efficiency was achieved with a relatively low adsorbent dosage under near-natural conditions and emphasised the potential of PRC850 as a sustainable and competitive alternative to chemically activated adsorbents in multi-metal wastewater treatment.

PRC850 was manufactured using a straightforward physical solution combustion technique that employed agricultural waste materials. This process offered several advantages, including the prevention of contamination from hazardous components, decreased energy and chemical usage, and reduced operational costs for water purification. The combination of high adsorption capacity, acceptable surface area, and eco-friendly production underlined the potential of PRC850 as a viable alternative to chemically activated carbons for the treatment of multi-metal contaminated water.

Several studies reported that chemical precipitation methods typically achieve Pb(II) removal rates of 70–90% under optimal pH and coagulant conditions [9], while membrane-based filtration systems could exceed 95% removal but were prone to fouling and high operational costs [65]. In contrast, the PRC850 biochar achieved up to 98.64% Pb(II) removal without chemical activation, under ambient conditions, and with significantly shorter equilibrium time than CGA. Moreover, compared to other bio-adsorbents such as coconut shell-based activated carbon (88%) and lignin-based porous carbon (96%) [31], PRC850 performed equally or more effectively. These results suggested that the adsorption method presented in this study was not only technically feasible but also highly promising for practical applications in water purification. Therefore, PRC850 should be selected for investigation into Pb(II) adsorption due to its extraordinary efficiency, which has not yet been recorded in the literature.

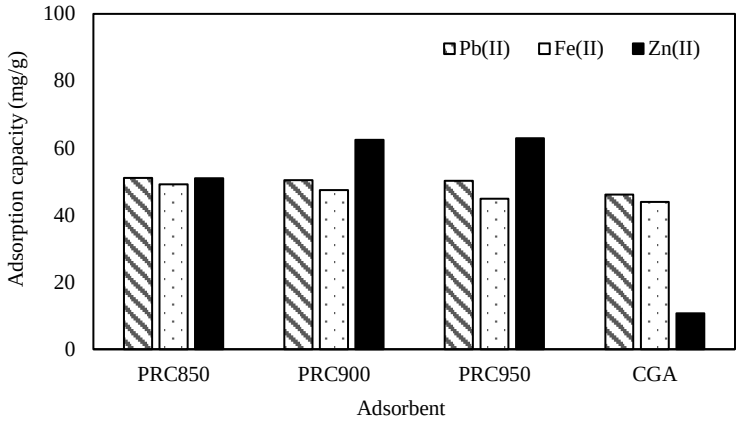


**Figure 9** Effect of different adsorbent on adsorption capacity of heavy metal ions

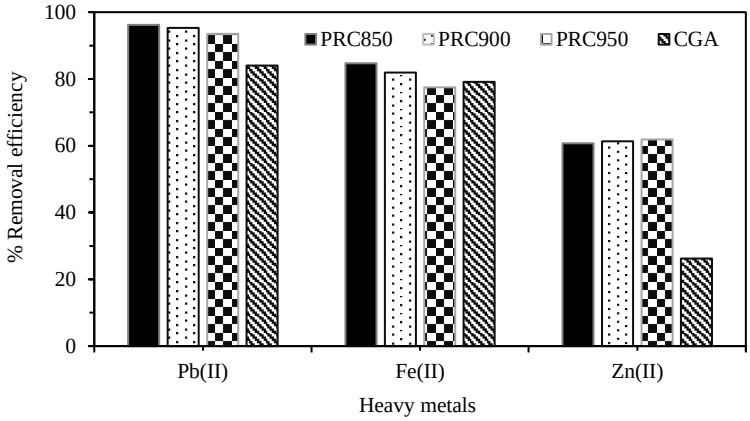


**Figure 10** Screening of adsorbents for heavy metal ion removal efficiency

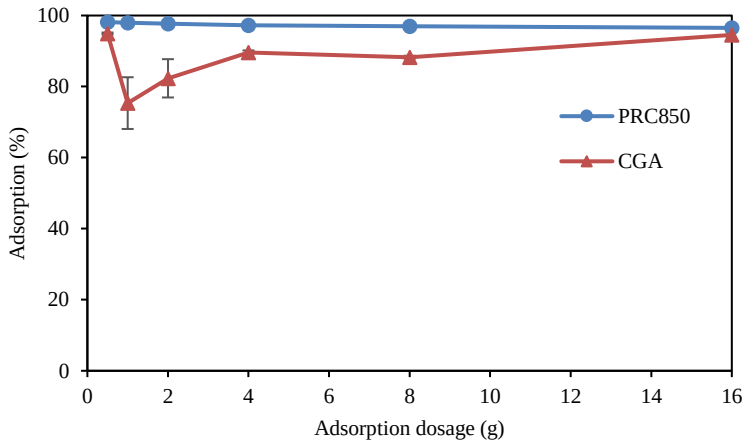


**Figure 11** Effect of adsorbent dosage of PRC850 on the adsorption of Pb(II) and CGA

*3.4 Effect of adsorbent dosage*

The influence of adsorbent dosage was recognised as a significant parameter affecting the adsorption of Pb(II). PRC850 was subsequently selected to examine the impact of adsorbent dosage due to its superior Pb(II) removal efficacy. The dose-dependent adsorption of Pb(II) on PRC850 and CGA adsorbents was studied by varying the amount of adsorbent (0.5, 1, 2, 4, 8, and 16 g) at a constant mass, using a 100 mL of 0.5 mg/L Pb(II) solution and shaking continuously (at 150 rpm) for 2 hours.

The data presented in Figure 11 illustrated the impact of varying the adsorbent dosage on the efficiency of Pb(II) adsorption. According to the data presented, all the dosages of the PRC850 adsorbent exhibited higher efficacy in adsorbing Pb(II) compared to CGA. The average adsorption rate for PRC850 was found to exceed 95%. The study revealed that the adsorption efficiency of PRC850 adsorbent at doses of 0.5, 1, 2, 4, 8, and 16 g was measured to be 98.13%, 98.01%, 97.71%, 97.28%, 96.94%, and 95.52%, respectively.

According to the findings, the level of Pb(II) adsorption was highest for PRC850 at a dose of 0.5 g, and declined steadily as the dose was increased up to 16 g. As depicted in Figure 11, the Pb(II) adsorption efficiencies decreased slightly as the PRC850 adsorbent dose increased, because equilibrium was attained in the contact surface area of adsorbent particles at 0.5 g.

Consequently, 0.5 g of PRC850 and CGA resulted in the highest Pb(II) adsorption efficiency. Nevertheless, increasing the PRC850 dosage beyond 0.5 g did not result in a statistically significant difference in adsorption efficiency, with only a marginal difference of 2.92%. The efficacy of Pb(II) adsorption was not enhanced by increasing the dosage of adsorbents beyond the steady state because there was already an abundance of excess adsorption sites compared to the sorbate. It was assumed that the number of adsorption sites per unit mass of adsorbents remained constant.

These behaviours are frequently encountered in adsorption processes, as documented in the existing literature [66]. A comparable study indicated that Cr(VI) adsorption efficiency reached 98% at 0.5 g of adsorbent, attained a steady state and subsequently dropped slightly by 0.6–0.7 g [41]. The study findings showed that the lowest dose of PRC850 adsorbent with the highest adsorption effectiveness was 0.5 g. Therefore, a quantity of 0.5 g of PRC850 adsorbent was selected for the subsequent study.

### *3.5 Effect of initial concentrations*

The study aimed to examine the adsorption of Pb(II) on PRC850 and CGA adsorbents at different concentrations. A 100 mL solution containing Pb(II) was prepared, with concentrations ranging from 0.25 mg/L to 8.00 mg/L. The adsorbents, weighing 0.5 g, were subjected to continuous shaking at 150 rpm for a duration of 2 hours. The findings are shown in Figure 12.

According to the data presented in Figure 12, it was observed that the percentage of Pb(II) adsorption by the PRC850 adsorbent exhibited a significant rise when the initial Pb(II) concentration in the solution was increased from 0.25 mg/L to 2.00 mg/L. Subsequently, the percent adsorption continued to increase gradually within the concentration range of 2.26 mg/L to 8.00 mg/L. The efficiency of Pb(II) adsorption demonstrated a steady rise as the initial concentration increased, eventually reaching a saturation point within the range of 2.00 mg/L to 8.00 mg/L. The adsorption capacity of the PRC850 adsorbent increased from 0.006 to 0.163 mg/g (81.05% to 98.64%) as the initial Pb(II) concentration rose. This increase could be attributed to the fact that the higher adsorbents have a higher concentration of Pb(II) ions per unit mass, which resulted in a greater rate of mass transfer of Pb(II) ions from the solution to the surface of the adsorbent. PRC850 and CGA adsorbents achieved the greatest Pb(II) adsorption efficiencies at 0.163 and 0.011 mg/g (98.64% and 85.52%) respectively. According to the results, the Pb(II) adsorption efficiency of PRC850 adsorbent exceeded that of CGA adsorbent.

Furthermore, it was observed that the percentage of Pb(II) adsorption by the CGA adsorbent declined as the initial Pb(II) concentration increased from 1 mg/L to 8 mg/L. Consequently, the efficiency of adsorption reduced significantly from 0.020 to 0.016 mg/g (82.39% to 9.34%.) The CGA adsorbents demonstrated adequate active sites to accommodate the limited Pb(II) ions at lower concentrations. However, when the concentrations of Pb(II) increased, the number of accessible sites for adsorption declined, resulting in a reduction in adsorption effectiveness for CGA adsorbents.

The improved mesoporosity and porous structure of PRC850 enabled enhanced Pb(II) absorption with increased starting concentrations, optimising the advantages of the concentration gradient. In contrast, CGA's compact structure and elevated bulk density (0.49 g/cm³) limited ion diffusion and restricted the availability of active sites. CGA rapidly reached saturation at low Pb(II) concentrations, and its efficacy declined at higher concentrations, despite optimal mass transfer conditions.

Moreover, the significant macroporosity of CGA provided minimal support for the adsorption of small ionic compounds such as Pb(II), owing to inadequate surface interactions within the larger pores. Conversely, the mesoporous structure of PRC850 facilitated multilayer adsorption, capillary condensation, and ion–surface interactions, leading to enhanced performance throughout the whole concentration range [49, 62, 67].

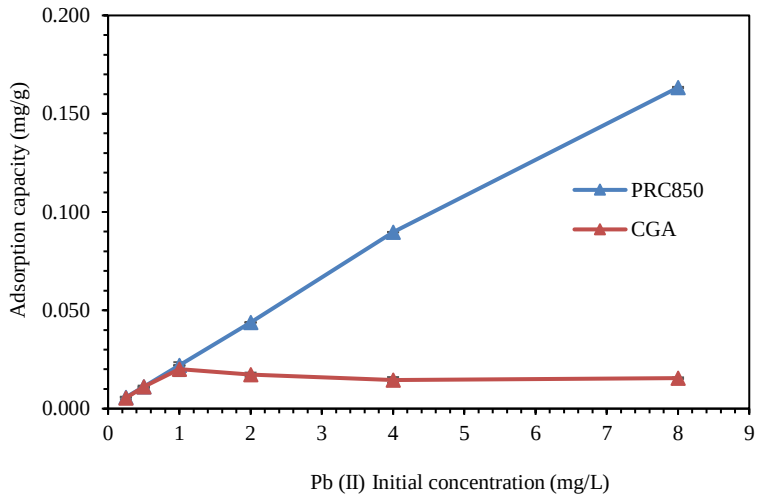


**Figure 12** Effect of initial concentrations on Pb(II) adsorption by PRC850 and CGA

### *3.6 Effect of contact time*

The influence of contact time was recognised as a significant parameter affecting the adsorption of Pb(II). The study investigated the adsorption of Pb(II) on PRC850 and CGA adsorbents across varying contact times of 0.5, 1, 2, 4, and 6 hours. The adsorbents were used at a fixed mass of 0.5 g, and a 100 mL solution containing 0.955 mg/L of Pb(II) was subjected to agitation at 150 rpm.

The data presented in Figure 13 illustrates the impact of contact time on the effectiveness of Pb(II) adsorption. According to the data, the Pb(II) adsorption efficiency of the CGA adsorbent increased with longer contact time. In contrast, the Pb(II) adsorption efficiency of PRC850 reached a saturation point and exhibited a minor decrease as contact time was prolonged. The CGA and PRC850 adsorbents exhibited removal efficiencies of 57.77% and 95.95% for Pb(II) within the initial 30-minute period, respectively. The

adsorption efficiency of Pb(II) by the PRC850 peaked at 96.75% after one hour. Subsequently, a minor decline in efficiency was observed over the 2 to 6-hour period, with a recorded value of 93.21% at the end of the 6-hour duration.

In contrast, the adsorption efficiency of Pb(II) by the CGA adsorbent reached its peak at 97.31% within a time frame of 6 hours, with adsorption equilibrium achieved after 4 hours. Based on the findings, the optimal contact time for adsorption onto PRC850 and CGA adsorbents was established as 1 hour and 4 hours, respectively. This determination was made due to the observation that the adsorption reached an equilibrium state after these specific durations. As a result, the rate of Pb(II) adsorption on PRC850 was initially rapid, followed by a gradual decrease due to the gradual reduction of accessible adsorption sites.

In general, the fast rates of adsorption, especially for CGA, were caused by the large number of active sites on the outside of the adsorbent that could interact with Pb(II). This fast rate occurred because, at the beginning, many empty surface sites were available for adsorption. After a certain period, the remaining empty surface sites became more difficult occupy due to repulsive forces between solute molecules in the solid and bulk phases [68]. Adsorbents with unoccupied active sites were easily accessible to anionic Pb(II) compounds in the solution, causing rapid adsorption at the initial stage. The slow transport of ions through pores and the electrostatic barrier generated by the adsorbent type may have impeded adsorption [69]. These behaviours are frequently encountered in adsorption processes, as documented in the existing literature [49, 67].

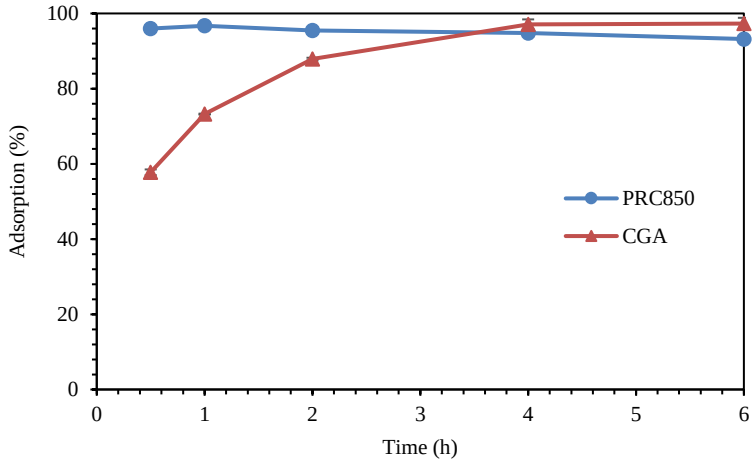


**Figure 13** Effect of contact time on Pb(II) adsorption by PRC850 and CGA adsorbents

*3.7 Adsorption isotherm and adsorption kinetics*

A number of models have been used to characterise adsorption isotherm data from experiments. Nonetheless, the Langmuir and Freundlich isotherms were the most widely used models [27, 49, 67]. The experimental results for Pb(II) adsorption on the adsorbents (PRC850 and CGA) were analysed using the Langmuir and Freundlich isotherm models (Figure 13). The Langmuir model demonstrated a high correlation coefficient ($R^2$ = 0.9581, as shown in Figure 12), while the Freundlich model exhibited a lower correlation coefficient ($R^2$ = 0.8393, also shown in Figure 12). This difference suggested that the adsorption of Pb(II) onto PRC850 was best represented by the Langmuir model.

It is worth noting that the Langmuir model exhibited the most favourable correlation coefficient values ($R^2$) in this study. Specifically, the $R^2$ values were determined to be 0.9581 for PRC850 and 0.3576 for CGA. The findings explicitly demonstrated that the adsorption of Pb(II) onto the adsorbents was most accurately described by the Langmuir model. The Langmuir model provided the best correlation and characterised the adsorption of Pb(II) on PRC850, which was indicative of a possible chemisorption process [67]. PRC850's superior Pb(II) adsorption capacity over CGA could be attributed to an adsorption mechanism involving a greater number of functional groups.

The data obtained from the experiment were analysed using the pseudo-second-order (PSO) kinetics model. The results for the PRC850 and CGA adsorbents are presented in Table 4 and Table 5, respectively. Pseudo-second-order model, depicted in Table 5 with a correlation coefficient ($R^2$) near 1, best explained the kinetics of Pb(II) adsorption on both PRC850 and CGA adsorbents. The $K_2$ values of PSO for the PRC850 and CGA adsorbents were 5.0579 and 4.8114, respectively.

In the pseudo-second-order model, adsorption capacity was assumed to be proportional to the number of active sites on the adsorbent surface [33], and the adsorption rate was considered to be governed by chemical adsorption.

**Table 4** Langmuir and Freundlich isotherm model for the adsorption of Pb(II) on PRC850 and CGA

| Absorbent | Langmuir | | | Freundlich | | |
|---|---|---|---|---|---|---|
| | $K_L$ (mg/g) | n | $R^2$ | $K_F$ (mg/g) | n | $R^2$ |
| PRC850 | 8.811 | 0.2901 | 0.9581 | 2.1865 | 0.1356 | 0.8393 |
| CGA | 0.2208 | 0.4138 | 0.3576 | 3.3896 | 1.7624 | 0.2508 |

**Table 5** The pseudo-second-order kinetic model of Pb(II) adsorption on PRC850 and CGA

| Absorbent | Kinetics | $K_2$ ($min^{-1}$) | $R^2$ |
|---|---|---|---|
| PRC850 | t/qt = 5.0579x – 0.2486 | 0.2486 | 0.9999 |
| CGA | t/qt = 4.8114x + 1.3809 | 1.3809 | 0.9985 |

## 4. Conclusions

This study successfully demonstrated the potential of rubber seed shells (RSS), an abundant agricultural by-product, to produce non-chemically activated biochar for heavy metal removal from aqueous solutions. The PRC850 adsorbent, produced via a simple two-step carbonisation process at 850 °C without any activating chemicals or gas input, was compared against a commercial-grade activated (CGA) carbon for its ability to remove Pb(II), Fe(II), and Zn(II).

PRC850 exhibited significantly superior performance in Pb(II) removal, with maximum efficiency reaching 98.13% at 0.5 g dosage, compared to 94.93% by CGA under the same condition. Notably, PRC850 maintained high removal efficiency even at higher initial concentrations, while CGA's performance declined sharply beyond 4 mg/L.

Furthermore, PRC850 achieved adsorption equilibrium in just 30 minutes, much faster than CGA, which required up to 240 minutes. This rapid adsorption aligned with the pseudo-second-order kinetic model ($R^2 > 0.99$), indicating chemisorption as the dominant mechanism.

Despite having a slightly lower BET surface area than CGA (795 $m^2/g$ vs. 925 $m^2/g$), PRC850 possessed a more favourable mesoporous structure (dominant pore range 3–8 nm), which enhanced the diffusion pathways for metal ions. In contrast, CGA exhibited a broader pore size distribution (17–138 nm) and lower adsorption density per surface area.

These findings were further supported by FTIR analysis: PRC850 retained key oxygen-containing functional groups (–OH, C=O, C–O) essential for metal binding, although some were thermally reduced, suggesting enhanced surface reactivity via partial carbon ordering. When compared with conventional treatment methods such as chemical precipitation, membrane filtration, and ion exchange—which often require high energy input, complex infrastructure, or hazardous chemicals—the use of PRC850 offered multiple advantages: simplicity of production, cost-efficiency, environmental sustainability, and operational safety. Its efficacy in multi-metal removal, low material cost, and chemical-free preparation made PRC850 an ideal candidate for decentralised or resource-limited wastewater treatment systems.

In summary, PRC850 outperformed CGA in terms of adsorption capacity, kinetics, and structural suitability. Its promising characteristics—derived from low-cost, non-toxic preparation—emphasised the value of agricultural waste conversion into functional adsorbents.

Future research should investigate long-term performance in continuous-flow systems, regeneration potential, and real wastewater applications to advance PRC850 as a sustainable solution for heavy metal remediation.

## 5. Acknowledgements

The research received financial support from Thailand Science Research and Innovation (TSRI) (No. FRB660030/0159/4263870). The authors acknowledge the support of the Faculty of Sciences and Health Technology at Kalasin University and the National Science and Technology Development Agency (NSTDA) for the provision of essential research facilities.

## 6. References

[1] Ahmed J, Thakur A, Goyal A. Chapter 1: Industrial wastewater and its toxic effects. In: Shah MP, editor. Biological Treatment of Industrial Wastewater. Cambridge: The Royal Society of Chemistry; 2021. p. 1-14.
[2] Chiamsathit C, Charin P, Thammarakcharoen S. Heavy metal pollution index for assessment of seasonal groundwater supply quality in rural area, Kalasin, Thailand. NU Int J Sci. 2020;17(1):45-60.
[3] Chiamsathit C, Auttamana S, Thammarakcharoen S. Heavy metal pollution index for assessment of seasonal groundwater supply quality in hillside area, Kalasin, Thailand. Appl Water Sci. 2020;10:142.
[4] Hung NV, Nguyet BTM, Nghi NH, Thanh NM, Quyen NDV, Nguyen VT, et al. Highly effective adsorption of organic dyes from aqueous solutions on longan seed-derived activated carbon. Environ Eng Res. 2023;28(3):220116.
[5] Amanze C, Zheng X, Man M, Yu Z, Ai C, Wu X, et al. Recovery of heavy metals from industrial wastewater using bioelectrochemical system inoculated with novel *Castellaniella* species. Environ Res. 2022;205:112467.
[6] Dutta D, Arya S, Kumar S. Industrial wastewater treatment: current trends, bottlenecks, and best practices. Chemosphere. 2021;285:131245.
[7] Department of Groundwater Resources. Groundwater quality survey and monitoring report. Bangkok: Ministry of Natural Resources and Environment; 2019. (In Thai)
[8] Mingkhwan R, Worakhunpiset S. Heavy metal contamination near industrial estate areas in Phra Nakhon Si Ayutthaya Province, Thailand and human health risk assessment. Int J Environ Res Public Health. 2018;15(9):1890.
[9] Fu F, Wang Q. Removal of heavy metal ions from wastewaters: a review. J Environ Manag. 2011;92(3):407-18.
[10] Jaishankar M, Tseten T, Anbalagan N, Mathew BB, Beeregowda KN. Toxicity, mechanism and health effects of some heavy metals. Interdiscip Toxicol. 2014;7(2):60-72.
[11] Pollution Control Department (PCD). Thailand state of pollution report 2021. Bangkok: Ministry of Natural Resources and Environment; 2022. (In Thai)
[12] Kongsricharoen N, Champa J, Kanjanasiranont N, Prueksasit T. Heavy metal contamination of surface water and groundwater from the waste electrical and electronic equipment (WEEE) recycling area in Buriram, Thailand. In: Jeon HY, editor. Sustainable Development of Water and Environment. ICSDWE 2020. Cham: Springer; 2020. p. 91-101.
[13] Chiamsathit C, Netkrut K. Assessment of heavy metal concentration in wastewater of silk dyeing in Kalasin, Thailand. Sci Eng Health Stud. 2021;15:1-7.
[14] Agency for Toxic Substances and Disease Registry (ATSDR). Toxicological profile for lead [Internet]. Atlanta: U.S. Department of Health and Human Services; 2007 [cited 2023 Sep 10]. Available from: Available from: https://www.atsdr.cdc.gov/toxprofiles/tp13.pdf.
[15] Muthuraman RM, Murugappan A, Soundharajan B. A sustainable material for removal of heavy metals from water: adsorption of Cd(II), Pb(II), and Cu(II) using kinetic mechanism. Desalin Water Treat. 2021;220:192-8.
[16] Borhan A, Hamidi MNR. Modification of rubber-seed shell activated carbon using chitosan for removal of $Cu^{2+}$ and $Pb^{2+}$ from aqueous solution. AIP Conf Proc. 2019;2157:020024.

[17] Abdel-Raouf MS, Abdul-Raheim ARM. Removal of heavy metals from industrial wastewater by biomass-based materials: a review. J Pollution Eff Cont. 2017;5(1):1-13.
[18] Saleh TA, Mustaqeem M, Khaled M. Water treatment technologies in removing heavy metal ions from wastewater: a review. Environ Nanotechnol Monit Manag. 2022;17:100617.
[19] Renu, Agarwal M, Singh K. Heavy metal removal from wastewater using various adsorbents: a review. J Water Reuse Desalin. 2017;7(4):387-419.
[20] Michaelis E, Nie R, Austin D, Yue Y. High surface area biocarbon monoliths for methane storage. Green Energy Environ. 2023;8(5):1308-24.
[21] Tong M, Lan Y, Yang Q, Zhong C. High-throughput computational screening and design of nanoporous materials for methane storage and carbon dioxide capture. Green Energy Environ. 2018;3(2):107-19.
[22] Zulkania A, Hanum GF, Rezki AS. The potential of activated carbon derived from bio-char waste of bio-oil pyrolysis as adsorbent. MATEC Web Conf. 2018;154:01029.
[23] Ademiluyi FT, Nze JC. Multiple adsorption of heavy metal ions in aqueous solution using activated carbon from Nigerian bamboo. Int J Res Eng Technol. 2016;5(1):164-9.
[24] Taha MF, Shuib AS, Shaharun MS, Borhan A. Removal of Ni(II), Zn(II) and Pb(II) ions from single metal aqueous solution using rice husk-based activated carbon. AIP Conf Proc. 2014;1621:210-7.
[25] Wanprakhon S, Sukcharoen P, Krongchai S. A comparative study of one-step and two-step activated carbon from longan seeds by dry chemical activation with NaOH. J Mater Sci Appl Energy. 2022;11(1):9-15.
[26] Mokti N, Borhan A, Zaine SNA, Zaid HFM. Development of rubber seed shell-activated carbon using impregnated pyridinium-based ionic liquid for enhanced $CO_2$ adsorption. Processes. 2021;9(7):1161.
[27] Tenev MD, Farías A, Torre C, Fontana G, Caracciolo N, Boeykens SP. Cotton industry waste as adsorbent for methylene blue. J Sustain Dev Energy Water Environ Syst. 2019;7(4):667-77.
[28] Mondal MK, Mishra G, Kumar P. Adsorption of cadmium (II) and chromium (VI) from aqueous solution by waste marigold flowers. J Sustain Dev Energy Water Environ Syst. 2015;3(4):405-15.
[29] Gaur N, Kukreja A, Yadav M, Tiwari A. Adsorptive removal of lead and arsenic from aqueous solution using soyabean as a novel biosorbent: equilibrium isotherm and thermal stability studies. Appl Water Sci. 2018;8:98.
[30] Boeykens SP, Saralegui A, Caracciolo N, Piol MN. Agroindustrial waste for lead and chromium biosorption. J Sustain Dev Energy Water Environ Syst. 2018;6(2):341-50.
[31] Yi H, Nakabayashi K, Yoon SH, Miyawaki J. Pressurized physical activation: a simple production method for activated carbon with a highly developed pore structure. Carbon. 2021;183:735-42.
[32] Yu M, Han Y, Li J, Wang L. $CO_2$-activated porous carbon derived from cattail biomass for removal of malachite green dye and application as supercapacitors. Chem Eng J. 2017;317:493-502.
[33] Ma C, Gong J, Zhao S, Liu X, Mu X, Wang Y, et al. One-pot green mass production of hierarchically porous carbon via a recyclable salt-templating strategy. Green Energy Environ. 2022;7(4):818-28.
[34] Dula T, Siraj K, Kitte SA. Adsorption of hexavalent chromium from aqueous solution using chemically activated carbon prepared from locally available waste of bamboo (*Oxytenanthera abyssinica*). ISRN Environ Chem. 2014;2014:438245.
[35] Gorbounov M, Petrovic B, Ozmen S, Clough P, Soltani SM. Activated carbon derived from biomass combustion bottom ash as solid sorbent for $CO_2$ adsorption. Chem Eng Res Des. 2023;194:325-43.
[36] The Nation. Thailand becomes world's top rubber exporter, China biggest buyer [Internet]. 2022 [cited 2022 Oct 11]. Available from: https://www.nationthailand.com/business/econ/40018839.
[37] Laskar MA, Ali SK, Siddiqui S. A potential bio-sorbent for heavy metals in the remediation of waste water. J Sustain Dev Energy Water Environ Syst. 2016;4(4):320-32.
[38] Thai Industrial Standard Institute. Thai industrial standard: activated carbon (TIS 900-2547). Bangkok: Thai Industrial Standard Institute; 2004. (In Thai)
[39] ASTM. ASTM D2867-23: Standard test methods for moisture in activated carbon. West Conshohocken: ASTM International; 2023.
[40] ASTM. ASTM D2866-11: Standard test methods for total ash content of activated carbon. West Conshohocken: ASTM International; 2018.
[41] Onyeji LI, Aboje AA. Removal of heavy metals from dye effluent using activated carbon produced from coconut shell. Int J Eng Sci Technol. 2011;3(12):8238-46.
[42] Wirtu YD, Melak F, Yitbarek M, Astatkie H. Aluminum coated natural zeolite for water defluoridation: a mechanistic insight. Groundw Sustain Dev. 2021;12:100525.
[43] ASTM. ASTM D4607-14: Standard test methods for determination of iodine number of activated carbon. West Conshohocken: ASTM International; 2021.
[44] Leng L, Huang H, Li H, Li J, Zhou W. Biochar stability assessment methods: a review. Sci Total Environ. 2019;647:210-22.
[45] Ekebafe LO, Imanah JE, Okieimen FE. Physico-mechanical properties of rubber seed shell carbon: filled natural rubber compounds. Chem Ind Chem Eng Q. 2010;16(2):149-56.
[46] Altıkat A, Alma MH, Altıkat A, Bilgili ME, Altıkat S. A comprehensive study of biochar yield and quality concerning pyrolysis conditions: a multifaceted approach. Sustainability. 2024;16(2):937.
[47] Lillo-Ródenas MA, Cazorla-Amorós D, Linares-Solano A. Understanding chemical reactions between carbons and NaOH and KOH. Carbon. 2003;41(2):267-75.
[48] Pinto PS, Silva RCF, de Freitas Filho RL, Santos LO, Pereira SD, Teixeira APC. Mesoporous carbon-based materials obtained from biomass and their application in the adsorption of contaminants: a review. J Braz Chem Soc. 2025;36(7):e-20250068.
[49] Kebede A, Kedir K, Melak F, Asere TG. Removal of Cr(VI) from aqueous solutions using biowastes: Tella residue and pea (*Pisum sativum*) seed shell. Sci World J. 2022;2022:7554133.
[50] Zhang C, Zhang Z, Zhang L, Li Q, Li C, Chen G, et al. Evolution of the functionalities and structures of biochar in pyrolysis of poplar in a wide temperature range. Bioresour Technol. 2020;304:123002.
[51] French AD, Cintrón MS. Cellulose polymorphy, crystallite size, and the Segal Crystallinity Index. Cellulose. 2013;20(1):583-8.
[52] Park S, Baker JO, Himmel ME, Parilla PA, Johnson DK. Cellulose crystallinity index: measurement techniques and their impact on interpreting cellulase performance. Biotechnol Biofuels. 2010;3:10.

[53] Yang H, Yan R, Chen H, Lee DH, Zheng C. Characteristics of hemicellulose, cellulose and lignin pyrolysis. Fuel. 2007;86(12-13):1781-8.
[54] Hosoya T, Kawamoto H, Saka S. Cellulose–hemicellulose and cellulose–lignin interactions in wood pyrolysis at gasification temperature. J Anal Appl Pyrolysis. 2007;80(1):118-25.
[55] Boateng AA, Mullen CA, Goldberg N, Hicks KB, Jung HJG, Lamb JFS. Production of bio-oil from alfalfa stems by fluidized-bed fast pyrolysis. Ind Eng Chem Res. 2008;47(12):4115-22.
[56] Marcus Y. Ion Properties. New York: Marcel Dekker; 1997.
[57] Stumm W, Morgan JJ. Aquatic chemistry: chemical equilibria and rates in natural waters. 3rd ed. New York: Wiley; 1996.
[58] Shannon RD. Revised effective ionic radii and systematic studies of interatomic distances in halides and chalcogenides. Acta Crystallogr A. 1976;32(5):751-67.
[59] Chen H, Yang X, Liu Y, Lin X, Wang J, Zhang Z, et al. KOH modification effectively enhances the Cd and Pb adsorption performance of N-enriched biochar derived from waste chicken feathers. Waste Manag. 2021;130:82-92.
[60] Wu Y, Li C, Wang Z, Li F, Li J, Xue W, et al. Enhanced adsorption of aqueous Pb(II) by acidic group-modified biochar derived from peanut shells. Water. 2024;16(13):1871.
[61] Fan D, Peng Y, He X, Ouyang J, Fu L, Yang H. Recent progress on the adsorption of heavy metal ions Pb(II) and Cu(II) from wastewater. Nanomaterials. 2024;14(12):1037.
[62] Wang A, Zheng Z, Li R, Hu D, Lu Y, Luo H, et al. Biomass-derived porous carbon highly efficient for removal of Pb(II) and Cd(II). Green Energy Environ. 2019;4(4):414-23.
[63] Zubair SA, Gaya UI. Adsorption of aqueous using granular adsorbents from *Accanthospermum hispendum* DC. J Sci Technol. 2021;13(1):18-29.
[64] ASTM. ASTM D2854-09: Standard test methods for apparent density of activated carbon. West Conshohocken: ASTM International; 2019.
[65] Barakat MA. New trends in removing heavy metals from industrial wastewater. Arab J Chem. 2011;4(4):361-77.
[66] Mekonnen E, Yitbarek M, Soreta TR. Kinetic and thermodynamic studies of the adsorption of Cr(VI) onto some selected local adsorbents. S Afr J Chem. 2015;68:45-52.
[67] Adane T, Haile D, Dessie A, Abebe Y, Dagne H. Response surface methodology as a statistical tool for optimization of removal of chromium (VI) from aqueous solution by Teff (*Eragrostis teff*) husk activated carbon. Appl Water Sci. 2020;10:37.
[68] Danish M, Hashim R, Rafatullah M, Sulaiman O, Ahmad A, Govind. Adsorption of Pb(II) ions from aqueous solutions by date bead carbon activated with $ZnCl_2$. Clean Soil Air Water. 2011;39(4):392-9.
[69] Karthikeyan T, Rajgopal S, Miranda LR. Chromium(VI) adsorption from aqueous solution by Hevea brasiliensis sawdust activated carbon. J Hazard Mater. 2005;124(1-3):192-9.